Non-equilibrium dynamics of magnetically anisotropic particles under oscillating fields

Steinbach, G.; Gemming, S.; Erbe, A.;

Originally published:

July 2016

European Physical Journal E 39(2016), 69

DOI: https://doi.org/10.1140/epje/i2016-16069-6

EPJ manuscript No.
(will be inserted by the editor)

Topical Issue: "Nonequilibrium Collective Dynamics in Condensed and Biological Matter"

Non-equilibrium dynamics of magnetically anisotropic particles under oscillating fields

Gabi Steinbach[1,2], Sibylle Gemming[1,2] and Artur Erbe[2]

[1] Institute of Physics, Technische Universität Chemnitz, 09107 Chemnitz, Germany.
[2] Helmholtz-Zentrum Dresden-Rossendorf, Bautzner Landstrasse 400, 01328 Dresden, Germany.

Received: date / Revised version: date

Abstract. In this article, we demonstrate how colloidal self-assembly and non-equilibrium dynamic processes can be enhanced by anisotropic particles. As an example, we study spherical particles with radially off-centered net magnetic moment in an oscillating field. Based on complementary data from a numerical simulation of spheres with shifted dipole and experimental observations from particles with hemispherical ferromagnetic coating, it is explained how this magnetic asymmetry gives rise to dynamic structural and orientational phenomena on a two-particle basis. We further present the behavior of larger ensembles of coated particles. It illustrates the potential for controlled reconfiguration based on the presented two-particle dynamics.

PACS. 45.20.dc Rotational dynamics – 45.50.Jf Few- and many-body systems – 82.70.Dd Colloids

1 Introduction

1.1 Motivation

Driving particle systems by time-dependent fields can induce a large variety of structural and dynamic phenomena [1,2]. The particular beauty and appeal of these processes lie in the fact that the behavior of interacting particles far away from equilibrium is often not intuitively comprehensible and contrasts strongly with the behavior under equilibrium conditions. Magnetic colloids are suitable mesoscale systems for the study of collective, non-equilibrium dynamics [3]. Remote and homogeneous control is feasible via external magnets, providing an unscreened interaction widely independent from environmental conditions such as temperature and pH-value. Further, the diversity of magnetic materials and synthetic fabrication methods enhances the pool of available building blocks [4–9] with respect to shape and magnetization distribution.

Studies of colloids under time-dependent fields have focused on two aspects, on the directed self-assembly of complex, reversible structures and on emergent dynamics [3]. Both result from the combination of the interaction of the particles with the field and the interparticle interaction, which is dominated typically by magnetic and hydrodynamic interactions. In present studies on non-equilibrium phenomena, primarily particles with isotropic magnetization distribution have been employed [10–13]. There, the wealth of observed and reported phenomena is controlled by the field parameters [3,14], such as intensity, direction and frequency, and/or the environment (surface/interface) [15,16].

In this paper, the possibility of symmetry breaking via particles with anisotropic magnetization distribution will be presented as a method to increase the available choice of tuning parameters. Anisotropic particles have already been studied efficiently in the context of complex structure formation under equilibrium conditions [7,17–23]. Here, we will show how the magnetic anisotropy provides novel types of dynamic behavior and directed self-assembly under time-dependent fields by magnetostatic interaction.

1.2 Magnetically anisotropic particles

An anisotropic magnetization distribution can be realized experimentally by, e.g., patchy particles [24] or so-called capped (Janus) particles [23,25,26], a sphere with hemispherical magnetic coating. Theoretical models assume a sphere with off-centered magnetic moment [27,28], e.g., a point dipole. As the key feature, the magnetic center in those particles is shifted away from their geometric center. This shift can have drastic consequences on the assembly behavior, since the the magnetic potential does not only

depend on the relative orientation between the particles but also on the distance between their magnetic centers. For particles with fixed net magnetic moment, two extreme cases have been reported, the one with the magnetic moment shifted laterally (Fig. 1 a) [27,29,30] and the one with a shift radially away from the particle center (Fig. 1 b) [28,25], but also intermediate cases exist [31,24]. Particles with a radial magnetic shift (Fig. 1 b) provide a particularly interesting assembly behavior. In equilibrium, they exhibit a non-parallel magnetic configuration (Fig. 1 c) [28,32,33], which is atypical for ferromagnetic systems. The same holds for particles with lateral shifts only in the case of large shifts. To our knowledge, those have not been in the focus of reports, yet, an will also not be studied here.

Any external field that is applied to particles with non-collinear magnetic order will align them and, thus, induce a change of the relative orientation angle. Due to the magnetic shift, this reorientation involves a change of the distance between the magnetic centers. Since the magnetic interaction is strongly distance dependent, the periodic change of the distance induced by time-dependent fields promises novel dynamic phenomena. So far, the dynamic behavior of ferromagnetically capped particles has been reported only for the case of an intermediate lateral shift [26], exhibiting collinear magnetic order. The behavior under rotating fields coincides with the one observed for isotropic ferromagnetic particles [12]. Both form planar compact clusters, and the hydrodynamic coupling of the rotating particles leads to an in-plane rotation of the clusters as a whole [26]. It should be noted that for the capped particles used in those studies more diverse assembly behavior occurs under precessing fields [34]. This is caused only by a soft-magnetic contribution of the utilized coating, giving rise to complex magnetization dynamics in the coating itself.

In this article, we focus on the more general, since material-independent, case of particles with fixed net moment provided by hard-magnetic materials. We will demonstrate how under oscillating fields the interaction between particles with radially shifted net magnetic moment exhibits unique dynamic phenomena and that this is comprehensible on the basis of the two-particle interaction. First, a numerical calculation based on the interaction of two dipolar particles will be presented. Afterwards, the findings will be substantiated by particles with a hemispherical hard-magnetic coating as an experimental realization of particles with radially shifted magnetization.

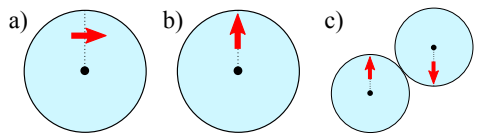

Fig. 1. Sketches of spherical particles with a fixed net magnetic moment (red arrow) that is shifted a) laterally or b) radially away from the particle center (black dot). c) Two particles with radial shift form a dumbbell with a non-collinear, antiparallel magnetic order.

2 Simulation: Oscillating sd-particles

2.1 Numerical system

The simplest model of a particle with a radially off-centered net magnetic moment is a sphere with embedded dipole that is shifted away from the particle center. The shift $\xi \in [0, ..., 1]$ (Fig. 2 a) is measured in particle radius r_p. So-called shifted-dipole particles (sd-particles) have already been studied intensively under equilibrium conditions [28, 33, 35]. As the principal result, the relative orientation between sd-particles in equilibrium depends on the value of ξ. Two particles in equilibrium align non-parallel for $\xi \geq 0.4$ and become (staggered) antiparallel for $\xi \geq 0.6$ (Fig. 1 c). To study the dynamics of particles with an antiparallel equilibrium orientation, in the investigations presented here a value of $\xi = 0.6$ is applied. The separate role of rotational motion by magnetostatic interaction under oscillating fields can be examined in a spatially fixed (non-deforming) cluster. Therefore, a dumbbell of two sd-particles p_1 and p_2 is considered. The absolute positions of both sd-particles are locally fixed at their geometric center in the xy-plane. The particles are free to rotate in any direction φ, θ (Fig. 2 a) such that the dipoles move on a sphere with a radius given by ξ.

For interacting particles $\mathrm{p}_{1,2}$ with shifted magnetic dipole $\mathbf{m}$ (unit vector $\hat{\mathbf{m}}$) and stray field $\mathbf{B}^\mathrm{p}$ that are exposed to an external field $\mathbf{B}^\mathrm{ex}$, the equation of rotation is obtained by balancing the rotational drag with the torques between the magnetic particles and between particles and the field. Note that due to the dipole shift, besides the aligning torque $\mathbf{m} \times \mathbf{B}^\mathrm{p}$, also the gradient force $(\mathbf{m} \cdot \nabla)\mathbf{B}^\mathrm{p}$ between the dipoles is relevant. Both convert into effective torques acting on the particles, such that

$$f_\mathrm{r} \dot{\Theta}(t) = \mathbf{m} \times \mathbf{B}^\mathrm{ex} + \mathbf{m} \times \mathbf{B}^\mathrm{p} + \xi \hat{\mathbf{m}} \times ((\mathbf{m} \cdot \nabla)\mathbf{B}^\mathrm{p}). \quad (1)$$

$\dot{\Theta}$ is the angular velocity of an object with rotational friction coefficient f_r and orientation $\Theta = (\theta, \varphi)$ (Fig. 2 a). An ensemble of n particles gives a system of n coupled equations of rotation given by Eq. 1, which can be solved numerically (appendix A).

An oscillating field $B^\mathrm{ex} = B_0^\mathrm{ex} \sin(\omega t)$ with angular frequency ω is applied normal to the assembly plane (Fig. 2 a). For two particles, we further define that the field points perpendicular to the plane spanned by the two dipoles in equilibrium. This assumption is based on the fact that in a planar assembly of dipolar particles all dipoles spontaneously lie in the assembly plane [36].

2.2 Interaction between two sd-particles

Starting with the field-free equilibrium state of two sd-particles, p_1 and p_2, where both dipoles adopt a staggered antiparallel configuration, an oscillating field B^ex perpendicular to the dipoles is switched on. The time-dependent trajectory of the dipoles is recorded in three-dimensions, given by angular (φ, θ) or spatial (x, y, z) coordinates (Fig. 2 a). Three features have been observed

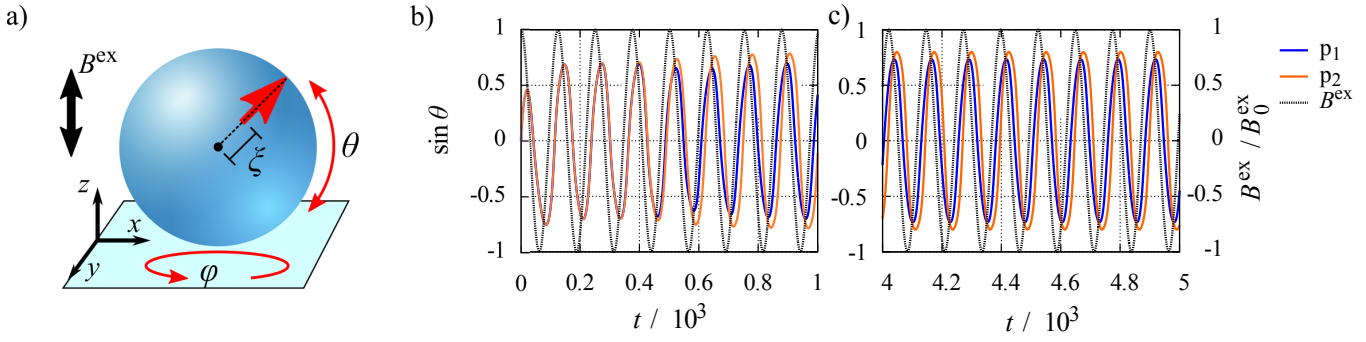

Fig. 2. a) The orientation of sd-particles with dipole shift ξ in the xy-assembly plane is given by the radial angle θ and the azimuthal angle φ. Oscillating fields B^{ex} are applied vertically (z-axis). b) Transient radial oscillation $\theta(t)$ (left axis) of two sd-particles p_1 and p_2 ($\xi = 0.6$) in contact after a field B^{ex} (right axis) is switched on and c) steady-state oscillation after some time.

that distinguish the behavior of sd-particles from those of normal dipolar particles. They are related to the radial oscillations $\theta(t)$ of both dipoles, the phase of $\theta(t)$ with respect to the field oscillation, and the azimuthal orientation φ. The latter is defined as the angle that is enclosed by the in-plane component of the dipole and the line connecting the particle centers.

First, the radial oscillation $\theta(t)$, parallel to the field direction, will be discussed. In Fig. 2 b, the radial oscillations $\theta(t)$ of p_1 and p_2 right after switching on the field is depicted. Initially, both dipoles oscillate uniformly with the same amplitude since they experience almost identical boundary conditions. Due to the frictional retardation, they lag behind the field oscillation $B^{ex}(t)$. With ongoing oscillations, the dipoles gradually obtain a relative phase shift and altered amplitudes θ_A. For p_1 the phase lag to $B^{ex}(t)$ and θ_A slightly decrease, and for p_2 both quantities increase. After a transient oscillation (here, ≈ 4000 time steps), the dipoles eventually obtain a steady-state oscillation (Fig. 2 c) with constant amplitude and phase lag that depend on the field amplitude B_0^{ex}. Note that the particles obtain different phase lags. The relative phase shift between the oscillations of the dipoles results from the interparticle interaction. This symmetry break can be understood only in the full picture of the steady-state dipole motion at different amplitudes B_0^{ex}, which will be presented next.

Three-dimensional steady-state trajectories of the dipoles of two interacting sd-particles have been recorded for a range of field amplitudes B_0^{ex} (Fig. 3 a). The amplitude $z_A = \xi \sin\theta_A$ of the radial oscillation, which is caused by the torque exerted by the external field, increases with B_0^{ex} [37]. Interestingly, the radial oscillation is accompanied by an azimuthal reorientation in the xy-plane. This is the second observed feature. The in-plane reorientation of the dipoles is clearly visible in the top view of the trajectories by projection onto the xy-plane (Fig. 3 b). With increasing field amplitudes B_0^{ex}, the dipoles gradually change from a staggered antiparallel configuration towards a collinear state. This can result from the dynamic interparticle interaction only, since this behavior is not obtained for two particles in a static field. The enforced periodic change of the radial orientation entails a periodic change of the distance and the angle enclosed between both shifted dipoles. Based on the anisotropic nature of dipole interaction, the sd-particles react by a gradual azimuthal reorientation until a field-dependent steady-state oscillation is reached.

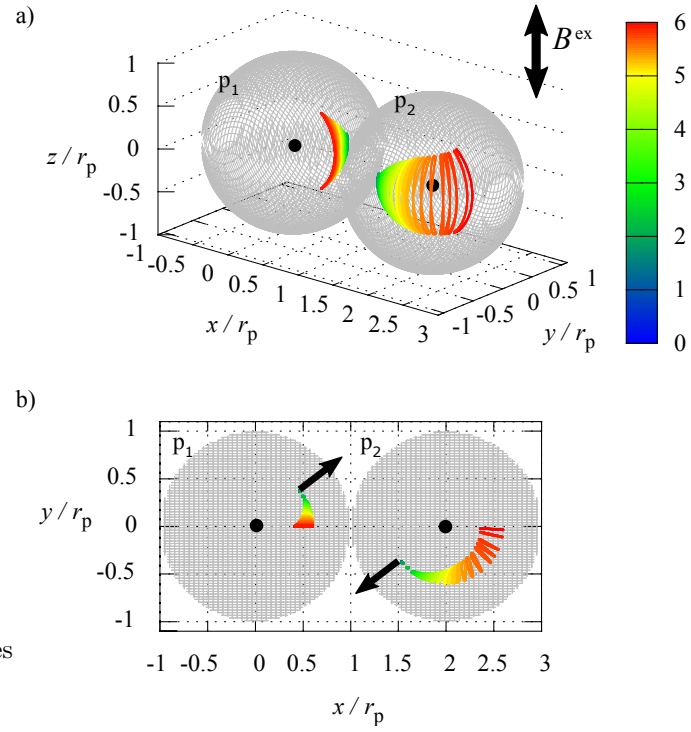

Fig. 3. Steady-state oscillations of two interacting sd-particles p_1 and p_1 ($\xi = 0.6$) in oscillating fields B^{ex} in **a**) a three-dimensional view and **b**) the top view. The trajectories display the trace of the dipole position. The color coding corresponds to the field amplitude B_0^{ex} measured in $\frac{\mu_0 m}{32\pi r_p^3}$.

The third feature becomes obvious by closer inspection of the steady-state trajectories at different values of B_0^{ex} (Fig. 4 a). They reveal that the in-plane orientation of the dipoles during one cycle of the oscillation is not

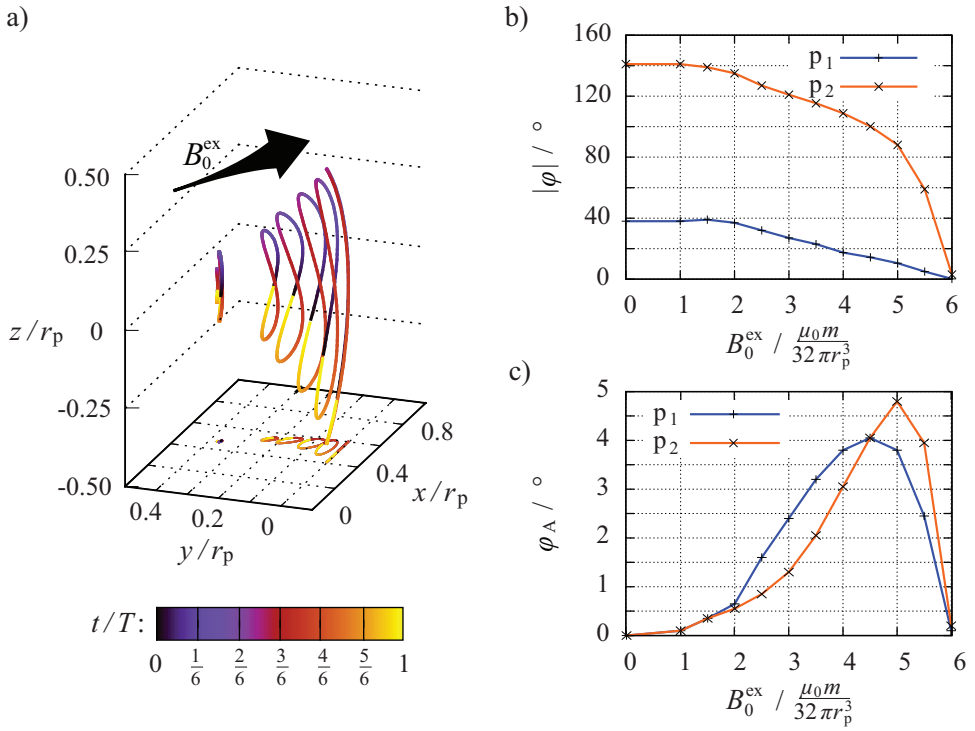

Fig. 4. Dependence of the steady-state oscillation of two interacting sd-particles ($\xi = 0.6$) on the field amplitude B_0^{ex}. **a**) Steady-state trajectories and their projections onto the xy-plane of the dipole in p_1 during one field cycle with period time T at different field amplitudes B_0^{ex}, from left to right: $B_0^{ex} = 1, 2, 3, 4, 5, 5.5,$ and $6\,\frac{\mu_0 m_p}{32\pi r_p^3}$. The trajectory is color coded according to the time of the field cycle, see color bar on the bottom. **b**) Absolute value $|\varphi|$ of the loop knot in the trajectory and **c**) in-plane oscillation amplitude φ_A of the dipoles in p_1 and p_2 as a function of the field amplitude, B_0^{ex}.

constant but periodically changes. The dipoles perform a trajectory in the form of a double loop. This is fascinating since it implies that under a uniaxial, oscillating field the two-particle interaction causes a periodic reorientation perpendicular to the field direction. The sense of direction of the loop is uniquely defined. This means that the dipoles follow a pathway that breaks time-reversibility.

The form and the location of the loop depend on the field amplitude B_0^{ex}. The form is described by its height, measured by the amplitude θ_A, and its width, the amplitude φ_A. In accordance with the above discussion, the radial amplitude θ_A increases with B_0^{ex} (Fig. 4 a). The in-plane position of the equilibrium oscillation loop of the dipole can be adjusted by B_0^{ex} as visible by the projection of the loops onto the xy-plane in Fig. 4 a. Here, the position is defined by the loop knot, which always lies in the assembly plane ($z = 0$). Its in-plane orientation φ is given by the angle that is enclosed by the center-to-loop knot vector and the line connecting the particle centers. Fig. 4 b shows that the absolute value $|\varphi|$ is a gradually decreasing function of the field intensity B_0^{ex} for both dipoles and $|\varphi|$ eventually converges to zero. The gradual in-plane reorientation implies that the dipoles experience a dynamic transition from an anti-parallel to a collinear orientation. In the example presented in Fig. 4 b, the latter is reached at about $B_0^{ex} = 6\,\frac{\mu_0 m_p}{32\pi r_p^3}$. It should be noted that for lower shift values ξ of the dipoles the curves will shift towards smaller field intensities B_0^{ex} since the values $|\varphi|$ in equilibrium decrease. Further, since φ correlates with θ, φ is also inversely proportional to ω. Consequently, increasing ω leads to a stretching of the curves in Fig. 4 b towards higher field amplitudes.

The width of the loop trajectory, φ_A, depends on B_0^{ex} in a non-monotonic way (Fig. 4 c). It becomes 0 (the width of the loop vanishes) either if the field vanishes (trivial case) or if the dipoles are already oriented in parallel ($\varphi_1 = \varphi_2$ at $B_0^{ex} > 6\,\frac{\mu_0 m_p}{32\pi r_p^3}$ for the example in Fig. 4 c). Between these limits the oscillation loop has a finite width that exhibits a maximum at a certain field value. In the presented example, the maximum occurs at around $B_0^{ex} \approx 5\,\frac{\mu_0 m_p}{32\pi r_p^3}$. With increasing dipole shift ξ the values (φ_A, B_0^{ex}) of the turning point increase as well. This finding suggests that the trajectory follows a non-reversal pathway (double loop) only below a critical field value, where $\varphi_A \neq 0°$, and becomes a reversible line trajectory otherwise. Since particles with centered dipole ($\xi = 0$) always align parallel they only perform such a line trajectory in oscillating fields. The loop trajectory is, thus, an effect that arises from the dynamic interaction of two particles with anisotropic magnetization distribution only.

3 Experiment: magnetically capped particles

3.1 Experimental particle system

Experimentally, particles with off-centered net magnetic moment have been realized by silica microspheres with hemispherical magnetic coating (appendix B). To obtain a stray field with dipolar character, exhibiting rotational and mirror symmetry, a hard-magnetic thin film ([Co/Pd] multilayers) with perpendicular magnetic anisotropy is deposited. The net magnetic moment of such a particle points parallel to the Janus director, such that the orientation of the net magnetic moment and the magnetic cap coincide.

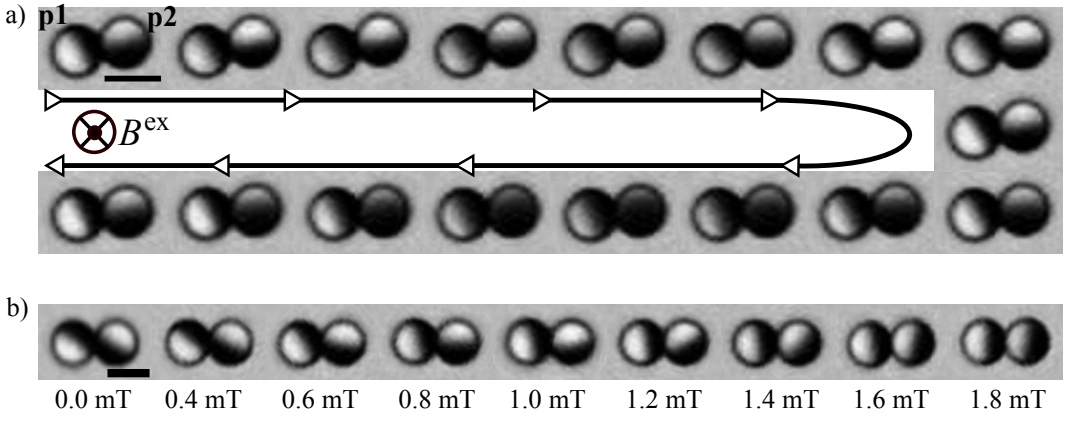

Fig. 5. Microscopy images of two capped particles in contact while exposed to an oscillating out-of-plane field B^{ex} ($\omega_B = 38\pi$ Hz). a) Time sequence during one field cycle ($B_0^{ex} = 0.7$ mT). b) Snapshots of two particles at different field amplitudes B_0^{ex} given below the images. (Scale bar: 5 μm)

Under an optical microscope, the contrast between the projected transparent silica hemisphere and the intransparent magnetic hemisphere visualizes the in-plane orientation of the net magnetic moment of such a particle [32]. The imaged projection of the transparent hemisphere vanishes for an out-of-plane orientation of the cap (either up or down) and becomes maximally visible for an in-plane orientation. Therefore, the size of the projected transparent hemisphere gives a measure for the radial angle θ of the net magnetic moment.

3.2 Two-particle interaction

In equilibrium, two such particles form a dumbbell where the caps have a staggered ($|\varphi_1 + \varphi_2| \neq 180°$) antiparallel orientation. A time-sequence of two such particles in contact under an oscillating field B^{ex} during one field cycle T has been recorded (Fig. 5 a). At first glance, one can see that the two particles do not oscillate uniformly as the sizes of their projected transparent hemispheres do not coincide in each frame. Specifically, the out-of-plane oscillation $\theta(t)$ of particle p_2 crosses the zero point (maximally visible transparent hemisphere) in the second image of Fig. 5 a, while the one of p_1 crosses the zero point in the first image. Thus, the oscillation $\theta(t)$ of particle p_2 lags behind the one of particle p_1. One can also see that particle p_1 oscillates with smaller amplitude since the minimum projected area of the transparent hemisphere is larger than the one of particle p_2. These findings are consistent with the results of the numerical investigation presented in Fig. 2 c.

As for the periodic change in the in-plane orientation of the particles, characterized by the width φ_A of the loop trajectory, the simulation suggests only small values. Experimentally, this oscillation cannot be resolved by the recorded microscopy movies since the error of the image analysis of about about $\pm 3°$ is on the same order of magnitude as φ_A.

In accordance with the numerical study, it can be detected that the relative orientation between two particles in an oscillating field depends on the field intensity. For different field amplitudes, we have extracted those snapshots during the oscillation where the caps obtain an almost in-plane orientation (Fig. 5 b). Starting from a state where the caps enclose an angle $\Delta\varphi = \varphi_1 - \varphi_2 = 180°$, they gradually change their relative orientation with increasing B_0^{ex}. The relative orientation, $\Delta\varphi$, decreases. A gradual transition from antiparallel to parallel in-plane orientation of the caps is achieved (Fig. 5 b).

3.3 Reconfiguration of particle assemblies

The relative reorientation between interacting capped particles from non-collinear to a collinear state can also be observed in larger particle assemblies under oscillating fields. If an equilibrium assembly deviates from a linear chain, the reorientation, additionally, can lead to a spatial reconfiguration of the assembly. This is attributed to the anisotropy of the magnetostatic interaction. The way of reconfiguration depends on the type of the structural pattern that exists in equilibrium. We have shown earlier that the capped particles self-assemble into two different structural patterns, staggered chains [32] and compact clusters [25], with non-collinear magnetic orientations. The observed configurations are a result of the magnetostatic interaction between the caps, providing an off-centered broad magnetization distribution. To demonstrate the dynamic reconfiguration as result of the relative reorientation in the particle-particle interaction under oscillating fields, selected examples of both structural patterns will be presented in the following (Fig. 6).

In a staggered chain in equilibrium, the caps obtain alternating orientations perpendicular to the chain direction. This means that net magnetic moments exhibit a staggered antiparallel magnetic orientation, which resembles the field-free arrangement of two particles (Fig. 5 b). Under oscillating fields perpendicular to the assembly plane, such staggered chains undergo a continuous transformation into linear chains (Fig. 6 a). This is visualized by the increasing staggering angle (red angle). The staggering transition is initiated by the reorientation of the caps. Based on the particle-particle interaction, neighboring particles undergo a transition from an antiparallel to a parallel configuration. Since each particle is connected to two neighbors in the chain, the collinear alignment of all particle-particle interactions can only be realized if the particles approach a linear chain. It can be assumed that the reorientation is supported by the magnetic interaction between

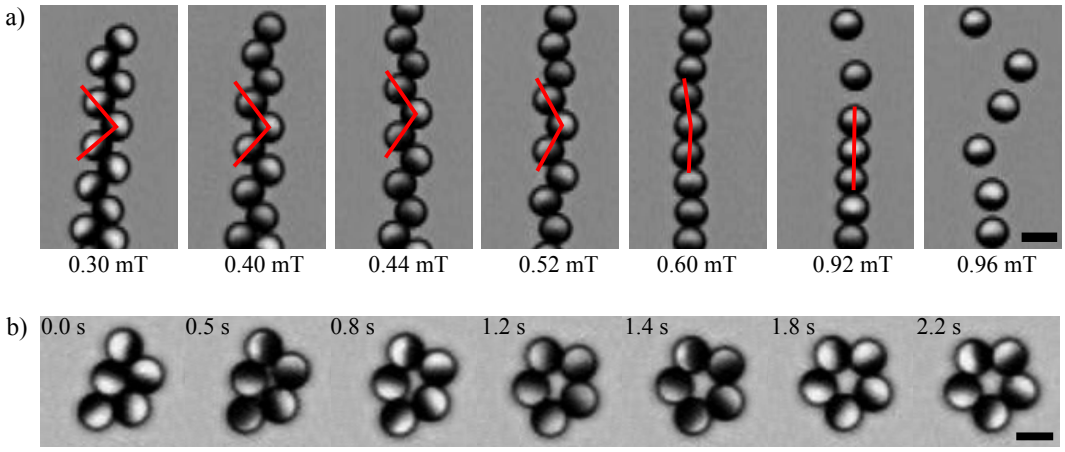

Fig. 6. Transformation of particle clusters while exposed to an oscillating out-of-plane field. a) Reversible expansion of a staggered chain under increasing field amplitudes B_0^{ex} as noted below the images ($\omega = 10\pi\,\mathrm{Hz}$). b) Time sequence of the abrupt transition of a compact cluster into a ring ($B_0^{\mathrm{ex}} = 1.6\,\mathrm{mT}$, $\omega = 38\pi\,\mathrm{Hz}$). The time is noted in the images. (Scale bar: $5\,\mu\mathrm{m}$)

next-nearest neighbors since two particles at farther distance prefer a parallel orientation. This can be understood from the fact that the relative offset of the net magnetic moment with respect to the interparticle distance becomes smaller for distant particles, leading to a preferred head-to-tail orientation [33].

The images in Fig. 6 a at different field intensities are steady-state configurations. The staggering angle is a unique function of the field amplitude B_0^{oop} at a constant field frequency. This means that the line can be expanded and contracted reversibly upon changing B_0^{oop}. Staggered chains rebuild from linear chains via the reorientation of the caps from parallel to antiparallel. Note, that above a critical field intensity the line breaks up into single particles if a critical angle θ^{cr} of the magnetostatic interaction is exceeded (last image in Fig. 6 a). Linear lines rebuild upon reducing B_0^{oop}, ensuring the reversibility of the transition. In contrast to the two-particle problem, particles within long chains have almost identical environments. Due to that the particles oscillate uniformly with coinciding amplitudes and no phase shift. Symmetry breaking is only present for particles at the end of the chains due to the lower coordination of the end particles. Qualitatively, this leads to non-uniform oscillations with different amplitudes and phase lag as described for the two-particle interaction (Fig. 2).

If the particles form compact clusters the response to oscillating fields differs from that of the staggered chain. The primary reason is that particles can have more than two (up to six) nearest neighbors. Therefore, it is impossible to obtain a gradual transition into a linear configuration between all nearest neighbors simultaneously. Some bonds between particles have to be broken up to obtain a collinear state. Below a critical field amplitude, the radial oscillation amplitude θ_A, which gradually increases with B_0^{oop}, is in the attractive regime of the interparticle interaction and the cluster remains stable. Above a critical field amplitude, where θ_A reaches the repulsive regime between neighboring particles, bonds can break up. Since θ_A of each particle depends on the local magnetic environment, the response of a cluster also depends on its exact magnetic configuration. For most cases, a sudden break-up of the cluster with immediate re-assembly into linear chains has been observed at a critical field amplitude. For a configuration as depicted in Fig. 6 b, the particles can also assume another metastable state. Above a critical field, an abrupt transition from a compact cluster into a ring has been observed (Fig. 6 b). Such a form minimizes the magnetostatic energy associated with the open ends of a linear chain on the cost of a non-zero angle between the magnetic moments of neighboring particles. This ring remains stable for an intermediate range of field amplitudes. It breaks up into single particles when the magnetostatic interaction between nearest neighbors becomes repulsive above a critical oscillation amplitude. Therefore, this structural transition has no linear dependency on the field amplitude. Either compact cluster form (low fields), rings form (intermediate fields) or the cluster disassembles into single particles (high fields).

4 Discussion and Conclusion

In this article, we have demonstrated that an anisotropic magnetization distribution in spherical particles causes unique dynamic phenomena when exposed to time dependent fields. We have presented numerical and experimental results on the rotational motion for the specific case of particles with a fixed net magnetic moment that is radially shifted away from the particle center, providing a stray field with dipole character. For two interacting particles under oscillating fields, three features have been detected that are not present for typical dipolar particles. First, the particles perform a non-uniform steady state oscillation in the external field by obtaining differing oscillation amplitudes and phase lags with respect to the external field. Second, the oscillation parallel to the field is accompanied by a relative reorientation between the particles perpendicular to the field direction. The equilibrium state of a staggered antiparallel orientation, a result of the shifted magnetization, gradually changes into a time-averaged collinear steady state with increasing field amplitudes. Third, in the steady state oscillation the dipoles perform a trajectory in the form of a double-loop as long as they do not reach the collinear state. The trajectory has a defined pass sense. This means

that for a non-collinear configuration these interacting particles break time-reversal symmetry under oscillating fields.

These findings suggest two additional control mechanisms for particle ensembles based on the two-particle interaction. First, orientational ordering can be manipulated by changing an external parameter that induces a transition from a non-collinear into a collinear state. Depending on the structure of an initial particle assembly, this can be realized by a gradual or an abrupt transition upon increasing the field intensity. Here, this has been demonstrated for two selected clusters with open and compact structures. For open structures, the gradual, controlled reorientation from non-collinear to collinear order might be of particular interest for applications with optically anisotropic particles [38]. Further, the relative reorientation of the particles is accompanied by a structural reconfiguration due to the anisotropy of the magnetic interaction. This possibility for structural reconfiguration of a particle assembly between dense/compact and linear structures gives the second control mechanism. While such a manipulation has been reported already previously for isotropic particles [39,40], the advantage in the presented mechanism lies in the reversibility of the transformation and the potential to couple orientational (optical) and structural ordering.

Finally, a universal impact of the presented numerical results on colloidal dynamics and self-assembly can be drawn since a very generic and simple model of a sphere with off-centered net magnetic moment has been exploited. For any particle system, a sufficiently large magnetic anisotropy can lead to an equilibrium configuration that deviates from the dipolar head-to-tail orientation. This non-collinear order is a prerequisite for the presented dynamics. Therefore, similar or comparable phenomena as presented in this article are expected to occur for any particles with shifted magnetization that exhibit a non-collinear equilibrium state. This article, thus, motivates further investigation using, for example, particles with lateral shifts [27], where the non-collinear state occurs for rather large shifts. Due to the different symmetry of those particles, the dynamic interaction under oscillating fields are expected to lead to other realizations of orientational and structural reconfiguration.

Appendix: Methods

Appendix A: Numerical calculation of the equation of rotation

The numerical calculation is based on the open source software 'compasses' [41], which calculates equilibrium states of fixed, finite size arrays of dipoles. Here, the code has been extended to implement the model of sd-particles where the dipole is radially shifted away by ξ from the spatially fixed center of the particles. The dipole is able to move as response to the stray field $\mathbf{B}^{\mathrm{d}}$ of other particles and to external fields $\mathbf{B}^{\mathrm{ex}}$. The motion is restricted to a sphere with a radius given by the value of the dipole shift ξ around the center of the particle. Additionally, the dipole always points normal to the surface of that sphere. Due to that any repositioning of the dipole on the sphere must result into a reorientation of the dipole and vice versa. Via the stray field $\mathbf{B}^{\mathrm{d}}$, one dipole $\mathbf{m}_1$ exerts an aligning torque $\tau^d = \mathbf{m} \times \mathbf{B}^{\mathrm{d}}$ on another dipole $\mathbf{m}_2$. For sd-particles with fixed positions, additionally, the gradient of the stray field of $\mathbf{m}_1$ exerts a translational force $\mathbf{F}^d = \mathbf{m}_2 \nabla \mathbf{B}_1^{\mathrm{d}}$ on $\mathbf{m}_2$. This force is converted into a torque $\tau^F = \xi \hat{\mathbf{m}} \times \mathbf{F}^d$ on the sd-particle. The equation of rotation of the sd-particles in a viscous environment, given by the torque balance (Eq. 1), is calculated iteratively. From the state at time t, the magnetic moment $\mathbf{m}_i$ of particle i at time step $t+1$ can be calculated by

$$\mathbf{m}_i^{(t+1)} = \mathrm{norm}\left[\mathbf{m}_i^{(t)} + \frac{1}{f_{\mathrm{r}}}(\tau^F + \tau^{\mathrm{d}} + \mathbf{m}_i \times \mathbf{B}^{\mathrm{ex}})\right] \quad (2)$$

The function 'norm[·]' scales the updated magnetic moments $\mathbf{m}^{(t+1)}$ to retain the initial magnitude m of the dipoles. In the calculation, a rotational friction coefficient of $f_{\mathrm{r}} = 100\,\frac{\mu_0 m^2}{32\pi r_{\mathrm{p}}^3}$ has been applied. Note that in the simulation the numerical time steps $\Delta t = (t+1) - t$ are dimensionless and set to 1. Therefore, the numerical friction coefficient f_r has the dimension of energy. To implement oscillating fields, the field intensity is recalculated after each iterative step t as $\mathbf{B}^{\mathrm{ex}} = \mathbf{B}_0^{\mathrm{ex}} \cos(\omega t)$. The angular frequency ω is also a dimensionless quantity and is set to 0.05.

Appendix B: Particle fabrication and experimental setup

The particle preparation and experimental setup has been described in detail in reference [32]. In short, silica spheres with a radius of $r_{\mathrm{p}} = (2.27 \pm 0.23)\,\mu$m have been coated by a $[\mathrm{Co}(0.28\,\mathrm{nm})/\mathrm{Pd}(0.9\,\mathrm{nm})]_8$ multilayer on one hemisphere via magnetron sputter deposition as described in reference [42]. Such a thin film has a perpendicular magnetic anisotropy. When deposited on the spheres, the stray field lines locally point perpendicular to the particle surface. This leads to the demanded stray field with dipolar character after magnetic saturation. A suspension of such particles in distilled water is studied via transmission light microscopy. Due to the density mismatch the particles sediment on the ground of the sample cell, providing a two-dimensional particle system. We have demonstrated previously [32] that the interaction between these particles on close contact is governed by magnetostatic interactions and other sources such as electrostatic interactions can be neglected. For the magnetic control, an electromagnetic coil is mounted parallel to the sample cell, providing low-frequency fields of up to 3 mT.

The authors are grateful to Manfred Albrecht and Dennis Nissen for the preparation of the colloidal particles. This work was supported by the German Research Foundation (DFG) via Grant No. ER 341/9-1, and FOR 1713 GE 1202/9-1.

References

1. M. C. Cross, P. C. Hohenberg, Rev. Mod. Phys. **65**, 851 (1993).
2. J. Dobnikar, A. Snezhko, A. Yethiraj, Soft Matter **9**, 3693 (2013).
3. J. E. Martin, A. Snezhko, Rep. Prog. Phys. **76**, 42 (2013).
4. S. H. Lee, C. M. Liddell, Small **5**, 1957 (2009).
5. C. H. Chen, A. R. Abate, D. Y. Lee, E. M. Terentjev, D. A. Weitz, Adv. Mater. **21**, 3201 (2009).
6. S. Sacanna, W. T. M. Irvine, L. Rossi, D. J. Pine, Soft Matter **7**, 1631 (2011).
7. P. Tierno, Phys. Chem. Chem. Phys. **16**, 23515 (2014).
8. S. C. Glotzer, M. J. Solomon, Nat. Mater. **6**, 557 (2007).
9. S. Q. Choi, S. G. Jang, A. J. Pascall, M. D. Dimitriou, T. Kang, C. J. Hawker, T. M. Squires, Adv. Mater. **23**, 2348 (2011).
10. P. Dillmann, G. Maret, P. Keim, Eur. Phys. J. ST **222**, 2941 (2013).
11. N. Osterman, I. Poberaj, J. Dobnikar, D. Frenkel, P. Ziherl, D. Babic, Phys. Rev. Lett. **103**, 228301 (2009).
12. S. Jäger, S. H. L. Klapp, Soft Matter **7**, 6606 (2011).
13. J. E. Martin, E. Venturini, G. L. Gulley, J. Williamson, Phys. Rev. E **69**, 021508 (2004).
14. P. Tierno, T. M. Fischer, T. H. Johansen, F. Sagues, Phys. Rev. Lett. **100**, 148304 (2008).
15. A. Snezhko, I. S. Aranson, W. K. Kwok, Phys. Rev. E **73**, 041306 (2006).
16. A. Snezhko, I. S. Aranson, Nat. Mater. **10**, 698 (2011).
17. A. Walther, A. H. E. Müller, Chem. Rev. **113**, 5194 (2013).
18. S. Jiang, J. Yan, J. K. Whitmer, S. M. Anthony, E. Luijten, S. Granick, Phys. Rev. Lett. **112**, 218301 (2014).
19. Q. Chen, S. C. Bae, S. Granick, Nature **469**, 381 (2011).
20. L. Hong, S. M. Anthony, S. Granick, Langmuir **22**, 7128 (2006).
21. J. Zhang, E. Luijten, S. Granick, Annu. Rev. Phys. Chem. **66**, 581 (2015).
22. G. R. Yi, D. J. Pine, S. Sacanna, J. Phys. Condens. Matter **25**, 193101 (2013).
23. A. B. Pawar, I. Kretzschmar, Macromol. Rapid Commun. **31**, 150 (2010).
24. S. Sacanna, L. Rossi, D. J. Pine, J. Am. Chem. Soc. **134**, 6112 (2012).
25. L. Baraban, D. Makarov, M. Albrecht, N. Rivier, P. Leiderer, A. Erbe, Phys. Rev. E **77**, 031407 (2008).
26. J. Yan, S. C. Bae, S. Granick, Adv. Mater. **27**, 874 (2015).
27. A. B. Yener, S. H. L. Klapp, Soft Matter **12**, 2066 (2016).
28. S. Kantorovich, R. Weeber, J. J. Cerda, C. Holm, Soft Matter **7**, 5217 (2011).
29. B. Ren, A. Ruditskiy, J. H. Song, I. Kretzschmar, Langmuir **28**, 1149 (2012).
30. J. J. Benkoski, J. L. Breidenich, O. M. Uy, A. T. Hayes, R. M. Deacon, H. B. Land, J. M. Spicer, P. Y. Keng, J. Pyun, J. Mater. Chem. **21**, 7314 (2011).
31. A. I. Abrikosov, S. Sacanna, A. P. Philipse, P. Linse, Soft Matter **9**, 8904 (2013).
32. G. Steinbach, D. Nissen, M. Albrecht, E. V. Novak, P. A. Sanchez, S. S. Kantorovich, S. Gemming, A. Erbe, Soft Matter **12**, 2737 (2016).
33. S. Kantorovich, R. Weeber, J. J. Cerda, C. Holm, J. Magn. Magn. Mater. **323**, 1269 (2011).
34. J. Yan, M. Bloom, S. C. Bae, E. Luijten, S. Granick, Nature **491**, 578 (2012).
35. M. Klinkigt, R. Weeber, S. Kantorovich, C. Holm, Soft Matter **9**, 3535 (2013).
36. T. A. Prokopieva, V. A. Danilov, S. S. Kantorovich, C. Holm, Phys. Rev. E **80**, 031404 (2009).
37. In this article, we analyze the dynamics as a function of the field amplitude B_0^{ex}, which increases concurrently with the oscillation amplitude θ_A. Alternatively, the results could be expressed as a function of the angular field frequency ω. In this case, the presented trends have to be inverted since θ_A decreases with increasing ω.
38. A. Fernandez-Nieves, G. Cristobal, V. Garces-Chavez, G. C. Spalding, K. Dholakia, D. A. Weitz, Adv. Mater. **17**, 680 (2005).
39. J. E. Martin, R. A. Anderson, R. L. Williamson, J. Chem. Phys. **118**, 1557 (2003).
40. A. Ruditskiy, R. Ren, I. Kretzschmar, Soft Matter **9**, 9174 (2013).
41. T. Nishimatsu. compasses at SourceForge.net, (2014). http://loto.sourceforge.net/compasses/. Accessed on March 18th 2016.
42. M. Albrecht, G. H. Hu, I. L. Guhr, T. C. Ulbrich, J. Boneberg, P. Leiderer, G. Schatz, Nat. Mater. **4**, 203 (2005).